JACS
JOURNAL OF THE AMERICAN CHEMICAL SOCIETY
Article
pubs.acs.org/JACS

Glutathione-Capped Gold Nanoclusters as Photosensitizers. Visible Light-Induced Hydrogen Generation in Neutral Water

Yong-Siou Chen and Prashant V. Kamat*

Radiation Laboratory and Department of Chemistry and Biochemistry, University of Notre Dame, Notre Dame, Indiana 46556, United States

Supporting Information

ABSTRACT: Glutathione-capped metal nanoclusters (Au_x-GSH NCs) which exhibit molecular-like properties are employed as a photosensitizer for hydrogen generation in a photoelectrochemical cell (PEC) and a photocatalytic slurry reactor. The reversible reduction (E^0 = −0.63 V vs RHE) and oxidation (E^0 = 0.97 and 1.51 V vs RHE) potentials of these metal nanoclusters make them suitable for driving the water-splitting reaction. When a mesoscopic TiO_2 film sensitized by Au_x-GSH NCs is used as the photoanode with a Pt counter electrode in aqueous buffer solution (pH = 7), we observe significant photocurrent activity under visible light (400−500 nm) excitation. Additionally, sensitizing Pt/TiO_2 nanoparticles with Au_x-GSH NCs in an aqueous slurry system and irradiating with visible light produce H_2 at a rate of 0.3 mmol of hydrogen/h/g of Au_x-GSH NCs. The rate of H_2 evolution is significantly enhanced (~5 times) when a sacrificial donor, such as EDTA, is introduced into the system. Using metal nanoclusters as a photosensitizer for hydrogen generation lays the foundation for the future exploration of other metal nanoclusters with well-controlled numbers of metal atoms and capping ligands.

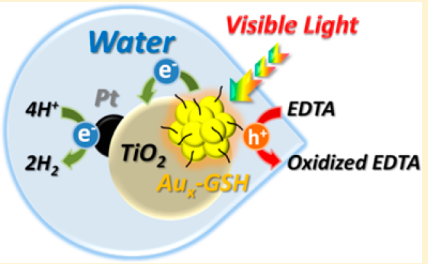

INTRODUCTION

Hydrogen is widely purported to be the fuel of the future. To realize this goal, it is necessary to develop a technology that can deliver hydrogen using renewable sources. The photocatalytic water-splitting reaction using semiconductor photocatalysts is considered to be one such viable option.[1] The large band gap semiconductors such as TiO_2 are quite effective, but lack response in the visible. Short band gap semiconductors such as CdS and CdSe can generate hydrogen from water only when there is a sacrificial electron donor present. Other visible light-absorbing semiconductors such as α-Fe_2O_3 require externally applied bias as high as 1.0 V.[2−4] Even though other semiconductors such as $BiVO_4$[5,6] and Si microwires[7] possess visible light-absorption properties resultant from their relatively small band gap, they are inactive toward water splitting reaction when used as a standalone system. In such a system, a *Z-scheme* photocatalytic system that couples a reductive and oxidative photocatalyst has been proposed to utilize two photons to induce water splitting.[8−10]

Sensitizing dyes such as porphyrins and Ru-complexes are often used to extend the photoresponse of large band gap semiconductor nanomaterials such as TiO_2.[11−13] To observe noticeable hydrogen production, it is necessary to couple these dyes with an oxygen-evolving catalyst or employ a sacrificial reagent to scavenge photogenerated holes.[13,14] Because of the stability issues of these systems under long-term operation, their usefulness toward practical applications remains a challenge.

Thiolated metal clusters have recently emerged as a new class of photosensitizers to extend the photoactivity of TiO_2. These gold and silver nanoclusters have few metal atoms in the core with bound thiol molecules in the shell. Their photophysical properties resemble the properties of molecular organometallic complexes.[15] In a recent study, we have shown that glutathione-capped gold nanoclusters (Au_x-GSH NCs) are capable of injecting electrons into TiO_2 under simulated solar illumination and can generate photocurrents in a metal cluster-sensitized solar cell with efficiencies comparable to that of CdS (2% power conversion efficiency).[16] Transient absorption spectroscopy measurements reveal a ligand-to-metal type excited-state transition with a 780 ns lifetime.[17] Since the photophysical properties of these metal nanoclusters can be tuned through their composition,[18−20] size,[21−24] and ligands,[25,26] they offer flexibility in photovoltaics and photocatalytic systems similar to semiconductor quantum dots. Another attractive feature of thiolated metal clusters is the metal core which can directly catalyze charge transfer processes. Previous studies have utilized Au NCs in catalytic systems, such as CO oxidation,[27−34] highlighting the catalytic properties of these NCs. The combination of photo and catalytic activity makes these metal nanoclusters an ideal choice for use in hydrogen production systems as they can serve as both photosensitizer and catalytic center.

To assess the photocatalytic properties of Au_x-GSH NCs and examine their potential use in water splitting, we have conducted photoelectrochemical and photocatalytic measurements with Au_x-GSH NCs modified TiO_2 films and nano-

Received: February 18, 2014
Published: March 26, 2014

   dx.doi.org/10.1021/ja5017365 | J. Am. Chem. Soc. 2014, 136, 6075−6082

particles (NPs). This maiden effort to utilize thiolated metal nanoclusters under visible light excitation for the generation of hydrogen highlights their potential for visible light solar fuel production.

EXPERIMENTAL SECTION

Chemicals. Gold(III) chloride trihydrate ($HAuCl_4 \cdot 3H_2O$, ≥99.9%, Sigma-Aldrich), chloroplatinic acid hexahydrate ($H_2PtCl_6 \cdot 6H_2O$, ≥37.5%, Sigma-Aldrich), L-glutathione reduced (≥98%, Sigma-Aldrich), ethylenediaminetetraacetic acid disodium salt, dihydrate (EDTA, 99+%, Sigma-Aldrich), sodium hydroxide (NaOH, ≥98%, Sigma-Aldrich), titanium tetrachloride ($TiCl_4$, 99.6%, Alfa Aesar), sodium phosphate monobasic ($NaH_2PO_4 \cdot H_2O$, Fisher), sodium phosphate dibasic (Na_2HPO_4, Fisher), acetonitrile (HPLC grade, Fisher), methanol (Certified ACS, Fisher). All chemicals were used as received without further purification.

Synthesis of Au_x-GSH NCs. Synthesis of Au_x-GSH NCs was adopted, with modification, from the literature report by Luo et al.[35] 0.24 g of gold(III) chloride trihydrate was dissolved in 300 mL deionized water (DI water) at room temperature in a 500 mL round-bottom flask. To this solution, was introduced 0.276 g of L-glutathione (under stirring) and stirred until the solution turned colorless; it typically took around 1.5 h. The flask was then heated to 70 °C in an oil bath with constant stirring. After 24 h, this flask was removed from the oil bath and allowed to cool to room temperature. The clusters were purified by adding 30 mL acetonitrile to 10 mL of the as-synthesized Au_x-GSH NC solution. This solution was mixed well and then centrifuged at 7800 rpm for 5 min. The supernatant was then discarded, and the remaining crystals were washed three times using a DI water and acetonitrile mixture (1:3 volume ratio). The purified Au_x-GSH NCs were dried under air flow and redispersed in DI water to a desired concentration (with the assistance of few drops of 0.5 M NaOH).

Cyclic Voltammetry of Au_x-GSH NCs. Cyclic voltammetry was performed using a three-electrode system. The counter electrode was platinum gauze, and the reference electrode was $Ag/AgNO_3$ (0.54 V vs RHE). The electrolyte was 0.1 M tetraethylammonium perchlorate (TEAP) in acetonitrile. The working electrode was prepared by dropping 200 μL of Au_x-GSH NCs solution onto a carbon paper (active area ∼0.8 cm^2, total area ∼4 cm^2) followed by drying under vacuum for 1 h at room temperature. The electrolyte was purged with N_2 in a sealed vial for 10 min prior to use. A suitable amount of electrolyte was used to ensure the active area was completely covered. N_2 gas was gently allowed to flow on top of the electrolyte interface during measurements. Potential was scanned from −1.4 to 1.4 V with an initial voltage of −0.8 V vs $Ag/AgNO_3$. The second scan was reported, and the voltage was reported vs RHE.

Preparation of Mesoporous TiO_2 Film. FTO (Pilkington TEC Glass-TEC 8, Solar 2.3 mm thickness) glass was washed in a detergent solution for 30 min in an ultrasonic bath followed by rinsing with DI water and ethanol. The films were then dried with a soft stream of air. A TiO_2-blocking layer was deposited by placing the plate into a 40 mM $TiCl_4$ aqueous solution at 70 °C for 30 min; it was then washed with DI water and ethanol and dried with a stream of air. The mesoporous TiO_2 film was deposited using the doctor blade technique (Solaronix, Ti-Nanoxide T/SP) with one layer of scotch tape as a spacer. This film was heated at 80 °C for 30 min and sintered at 500 °C for 1 h. The TiO_2 film was again treated with 40 mM aqueous $TiCl_4$ at 70 °C for 30 min, washed with DI water and ethanol, dried with a gentle stream of air, and finally sintered at 500 °C for 30 min. The film thickness was approximately 3.6 μm as measured by a profilometry (DektakXT, Bruker).

Sensitization of Au_x-GSH NCs on Mesoporous TiO_2 Film. The TiO_2 electrode was immersed into an Au_x-GSH NCs solution (4.6 wt %, pH ≈ 4, adjusted by NaOH or acetic acid) and kept at room temperature for 24 h. The Au_x-GSH-sensitized TiO_2 electrode was then washed thoroughly with DI water and ethanol and dried under a stream of air.

Measurement of Photocurrent from Photoelectrochemical Cell (PEC). A two-electrode system was used to measure the photocurrent generated from TiO_2 or Au_x-GSH-sensitized TiO_2 electrode (0.9 cm × 2 cm active area on 0.9 cm × 5 cm FTO). A three-armed cell was used where one arm was sealed with a rubber septum. Platinum gauze was employed as the counter electrode. Prior to measurement, the electrolyte was purged with nitrogen for 15 min to achieve an oxygen-free environment. Nitrogen gas was gently flowed above the electrolyte interface during all the measurements. A 300 W xenon lamp was used as a light source and coupled with a 420 nm cutoff filter. The electrochemical cell was placed at an appropriated position to achieve a 300 mW/cm^2 visible illumination. The power of illumination was calibrated using a power meter (Scientech 360001 as a head and Scientech 365 as a meter). Back-side illumination (glass side) was employed in all measurements. A Princeton Applied Research model PARSTAT 2263 was used to record photocurrent. Photocurrent density was reported by dividing the photocurrent obtained from each experiment by the illumination area (0.286 cm^2).

Measurement of Incident Photon to Charge Carriers Efficiency (IPCE) from PEC. IPCEs of TiO_2 and Au_x-GSH-sensitized TiO_2 photoanode were measured using a setup similar to that described above. A monochromator was placed in front of the xenon lamp to allow for the selection of a desired wavelength of monochromatic light. The irradiation power density was measured using a photodiode with a precalibrated current-to-power conversion factor at each wavelength. The power density at each wavelength was typically between 1.8 and 4.3 mW/cm^2. The photocurrent was recorded at short-circuit current conditions with the illumination wavelength tuned from 350 to 600 nm at 10 nm increments. IPCE was calculated using the following equation:

$$\mathrm{IPCE}(\%) = \frac{1240 \times \text{photocurrent density}(\mathrm{mA/cm^2}) \times 100}{\text{wavelength}(\mathrm{nm})/\text{power density}(\mathrm{mW/cm^2})}$$

Measurement of Hydrogen Generation from PEC. A 7 cm^2 (3.5 cm × 2 cm) TiO_2 film was deposited on an 8 cm^2 FTO (4 cm × 2 cm). Silver paste (590-G, generously given by ESL ElectroScience) was used to connect the bare FTO with a platinum wire and was sintered at 450 °C for 1 h. After cooling down to room temperature, the contact area was sealed using epoxy (Hysol 1C). The electrode was then sensitized with Au_x-GSH NCs. The edge of the electrode was sealed using epoxy (See Figure S2A in the Supporting Information [SI]). A custom-built cell made of Pyrex glass was used (see Figure S2B in the SI). Platinum gauze was employed as the counter electrode, and 11 mL of 0.1 M phosphate solution (pH = 7) with or without 0.1 M EDTA was employed as electrolyte (The electrolyte containing EDTA was adjusted to pH = 7 using NaOH). Prior to the measurement, the electrolyte was purged with ultrapure Argon gas for 15 min. A 300 W xenon lamp with a 420 nm cutoff filter coupled with a 13 cm long water filter was used as a light source. The electrochemical cell was placed at an appropriated position to achieve a 300 mW/cm^2 visible illumination. Back side illumination (glass side) was employed. 40 μL of the headspace (∼4 mL) was injected into GC (Thermo Scientific, Trace GC Ultra Gas Chromatographs with TCD detector and molecular sieves 5Å column, argon as a carrier gas) through a gastight syringe (50 μL, series A-2 syringe, Valco) at the desired sampling time. Calibration curves were established using known amounts of gases. The amount of hydrogen reported in Figure 3B herein and in Figure S4B in the SI are the detected amounts of H_2 multiplied by 100 since the volume of the headspace is 100 times greater than the sample volumes injected into GC.

For the two-electrode system shown herein, photocurrent was recorded under short circuit conditions For the three-electrode system shown in the SI, photocurrent was recorded under an external bias of 0.4 V vs RHE (reference electrode: Ag/AgCl (saturated KCl)). The applied bias can be converted using the equation below:

$$\text{applied bias}(\text{vs RHE}) = \text{applied bias}(\text{vs } [\mathrm{Ag/AgCl(saturated\ KCl)}]) + 0.197 + \mathrm{pH} \times 0.059$$

dx.doi.org/10.1021/ja5017365 | J. Am. Chem. Soc. 2014, 136, 6075−6082

Synthesis of Pt Loaded TiO_2 Nanoparticles (Pt/TiO_2 NPs). Pt/TiO_2 NPs were synthesized, with some modification, by photodeposition following a method described previously in the literature.[41] In this synthesis, 0.2 g of TiO_2 (Degussa, P25) was placed in a 250 mL round-bottom flask containing 160 mL of DI water and 40 mL of methanol; 0.75 mL of 4.18 mM $H_2PtCl_6{\cdot}6\,H_2O$ aqueous solution was added to achieve a 0.3 wt % of Pt loading ($Pt/(Pt+TiO_2) \times 100\%$). The flask was then sealed and sonicated for 10 min followed by stirring under nitrogen bubbling for 1 h. Photodeposition was carried out by placing a 13 cm long water filter and the flask in front of a 300 W xenon lamp. The flask was kept in front of the lamp for 2 h with continuous stirring. Nitrogen gas was gently flowed over the headspace during the entire deposition process. The resulted Pt/TiO_2 NPs were then washed with DI water and ethanol, and dried at 70 °C for 1 h.

Sensitization of Au_x-GSH NCs on Pt/TiO_2 NPs. Into a 10 mL Au_x-GSH NCs solution (4.6 wt %, pH ≈ 4, adjusted by NaOH or acetic acid) was added 0.15 g of Pt/TiO_2 NPs. The solution was stirred for 4 h at room temperature. The Au_x-GSH-sensitized Pt/TiO_2 NPs were then isolated by centrifugation, washed with ethanol, and dried under nitrogen flow overnight. The loading of Au_x-GSH NCs on Pt/TiO_2 NPs (calculated as ∼18 wt %) was determined by measuring the weight difference before and after sensitization.

Measurement of Hydrogen Generation from Photocatalytic Slurry System. Fifteen mg of Au_x-GSH-sensitized Pt/TiO_2 NPs or Pt/TiO_2 NPs were first dispersed into 6 mL of DI water (pH = 7.0, adjusted by NaOH) or 0.01 M EDTA (pH = 7.0, adjusted by NaOH) by sonication. Next, 4 mL of this solution (containing 10 mg of Au_x-GSH-sensitized Pt/TiO_2 NPs or Pt/TiO_2 NPs) was transferred to a ∼4.5 mL quartz cuvette (1 cm path length). This reaction cell was then sealed with a rubber septum, and ultrapure Argon gas was bubbled through the cell for 15 min prior to the measurement. A 300 W xenon lamp, a 420 nm cutoff filter, and a 13 cm water filter were employed. The reaction cell was placed at an appropriated distance from the illumination source to achieve 300 mW/cm^2 visible illumination. Forty μL of the headspace (∼0.5 mL) was injected into GC through a gastight syringe at the desired time intervals. The amount of hydrogen reported in Figure 6 herein and the estimated apparent quantum yield (AQY) were the results after multiplying by 12.5 since the volume of headspace is 12.5 times greater than the sample volume injected into GC.

AQY was measured using an LED flashlight (395 nm, LEDwholesales) after 6 h of illumination. The power density (∼2.57 mW/cm^2) was measured using a calibrated photodiode described in earlier section. The AQY was calculated by the equation:

$$\mathrm{AQY}(\%) = \left(\frac{\text{number of reacted electrons}}{\text{number of incident photons}}\right) \times 100\%$$

$$= \left(\frac{\text{number of evolved } H_2 \times 2}{\text{number of incident photons}}\right) \times 100\%$$

General Characterizations. Absorption spectra were measured using a Varian Cary 50-Bio UV−vis spectrophotometer. Emission spectra were recorded using a Horiba Fluorolog spectrometer. TEM images were taken using FEI Titan 80-300 microscope under 300 kV with Gatan Image Filter.

RESULTS AND DISCUSSION

Au_x-GSH/TiO_2 Photoanode of PECs for Water Splitting Reaction. The Au_x-GSH nanoclusters employed in this study were synthesized following an earlier published report.[16,35] The absorption spectrum of Au_x-GSH clusters is shown in Figure S1 in the SI. These Au_x-GSH nanoclusters were deposited onto mesoscopic TiO_2 films by immersing the film in an aqueous Au_x-GSH NC suspension (pH = 4) for 24 h. The interaction between carboxylic acid groups of the Au_x-GSH NCs and the TiO_2 surface seem to facilitate deposition at this slightly acidic pH.[36] After soaking the TiO_2 film in the NC solution, the film turns yellow in color, confirming the attachment of the Au_x-GSH nanoclusters. The absorption spectrum of Au_x-GSH-TiO_2 film (spectrum (b) in Figure 1A) shows absorption characteristics similar to that of the Au_x-GSH NCs in solution with an absorption onset at ∼520 nm and a shoulder at ∼400 nm. These absorption features of Au_x-GSH nanoclusters confirm the loading of the sensitizer on the TiO_2 surface. The absorption onset at 520 nm corresponds to an optical transition of 2.38 eV.

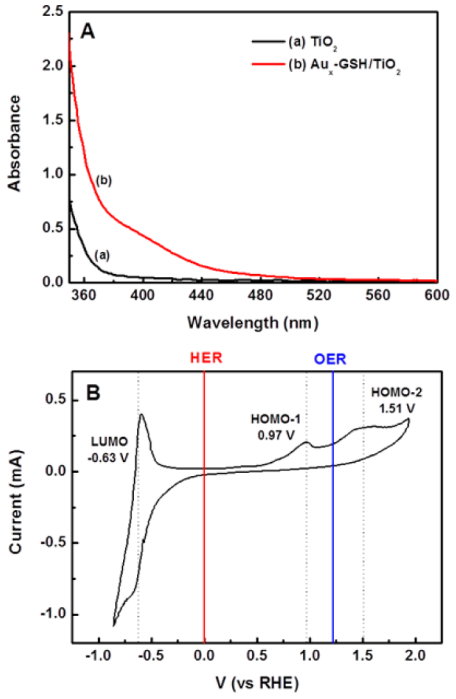

Figure 1. (A) Absorption spectra of (a) TiO_2 film and (b) Au_x-GSH sensitized TiO_2 film deposited on conducting glass electrodes. (B) Cyclic voltammogram of Au_x-GSH NCs deposited on carbon paper (electrolyte: degassed acetonitrile containing 0.1 M tetrabutyl ammonium perchlorate). Reference potentials, HER: potential of hydrogen evolution reaction at pH = 0; OER: potential of oxygen evolution reaction at pH = 0.

To further assess the redox properties of these Au_x-GSH NCs, we conducted cyclic voltammetry experiments by depositing Au_x-GSH NCs on a carbon electrode. The acetonitrile medium employed in the electrochemical experiment enabled a wider electrochemical window to assess the redox peaks. The cyclic voltammogram (Figure 1B) shows a reduction potential of −0.63 V and two oxidation potentials at 0.97 and 1.51 V (vs RHE). In the case of colloidal semiconductors such reduction and oxidation peaks are used to determine the position of conduction and valence bands (or LUMO and HOMO). If we consider the reduction peak and first oxidation peak of the Au_x-GSH NCs as the LUMO and HOMO energy levels, we obtain an energy gap of 1.6 eV for the first transition, and 2.14 eV when considering the second oxidation peak. The second transition value is close to the value obtained from the optical absorption spectra. On the basis of the solar flux and the energy gap for Au_x-GSH NCs one can expect a maximum theoretical limit for solar to fuel conversion efficiency of ∼10%.[37,38]

What we observe are two quasi-reversible peaks at 0.97 and 1.51 V vs RHE in acetonitrile (neutral). If these values hold good for pH 7, we expect the potential for water oxidation still

dx.doi.org/10.1021/ja5017365 | J. Am. Chem. Soc. 2014, 136, 6075−6082

to be thermodynamically favorable (E_{ox} (H_2O) = 0.81 V at pH 7). If the overvoltage required for water oxidation is relatively high, the first oxidation potential seen at 0.97 V may limit the water oxidation at Au_x-GSH NC. To check the validity of this hypothesis we conducted a series of photoelectrochemical experiments in the absence and presence of a sacrificial electron donor.

The Au_x-GSH NCs-coated TiO_2 electrode was used as a photoanode in a photoelectrochemical cell (PEC) with a platinum cathode. Figure 2A shows the incident photon-to-charge carrier efficiency (IPCE) of this PEC with monochromatic light illumination. Subsequent measurements were carried out with this two-electrode configuration under short circuit conditions using N_2-saturated phosphate buffer (pH = 7) with and without EDTA. The IPCE spectral response clearly shows the visible activity arising from Au_x-GSH NCs. Unmodified TiO_2 films showed no photocurrent response in the visible (>400 nm) because of requirement of high-energy excitation (band gap of anatase TiO_2, 3.18 eV). Upon sensitizing TiO_2 with Au_x-GSH NCs, the photoanode exhibited a photocurrent onset at ~520 nm (trace (c) in Figure 2A), which matches well with the absorption features of the Au_x-GSH-sensitized TiO_2 photoanode (Figure 1A). In a separate experiment we also introduced 0.1 M EDTA into the electrolyte to see its effect on interfacial hole transfer. IPCE spectra show an increased efficiency response upon introduction of EDTA into the electrolyte. For example, IPCE at 420 nm increased over 60% from 2.9% to 4.8% when 0.1 M EDTA was present in the electrolyte ((d) in Figure 2A).

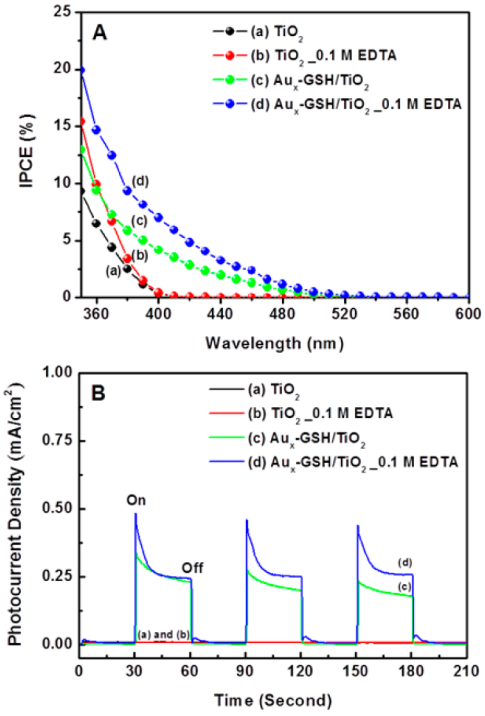

Figure 2. (A) Photocurrent action spectrum (IPCE) and (B) photocurrent density response to on−off cycles of illumination of photoanodes: (a) and (b) TiO_2; (c) and (d) Au_x-GSH-sensitized TiO_2 in the (a,c) absence and (b, d) presence of 0.1 M EDTA. Experimental conditions: Two electrode configuration using platinum gauze as a counter electrode; 0.1 M N_2 saturated phosphate solution (pH = 7) as electrolyte. Traces in (B) were recorded using 300 mW/cm^2 visible illumination from a xenon lamp with a 420 nm cutoff filter.

The photocurrent response in the visible region confirms that the origin of the photocurrent lies in the excitation of Au_x-GSH nanoclusters. Although the observed IPCE maximum is rather low (<10%) because of low fractional absorption of incident light, the results in Figure 2A confirm the ability of excited Au_x-GSH NCs to inject electrons into TiO_2 and thus serve as a visible sensitizer (eqs 1−3) for water splitting. Lower IPCE in the absence of EDTA (hole scavenger) in the electrolyte shows that the water oxidation remains a limiting factor at the photoanode.

The principle of Au_x-GSH NCs-sensitized PEC for the water-splitting reaction is presented in Scheme 1A. As shown in our earlier study, photoexcited Au_x-GSH NCs are capable of injecting electrons into TiO_2 (eqs 1 and 2).[16] The electrons transferred to the Pt counter electrode through the external circuit are energetic enough to enable hydrogen evolution (eqs 3 and 4). The Au-GSH$^+$, formed upon electron injection into TiO_2, must be reduced so that the sensitizer is regenerated. Given the relatively high oxidation potential of Au_x-GSH, oxidation of water by Au-GSH$^+$ (eq 5) should be possible. If this regeneration step does not take place, one would expect self-oxidation (eq 6), resulting in the net loss of the sensitizer.[39,40]

$$Au_x - GSH \xrightarrow{h\nu} Au_x - GSH^* \quad (1)$$

Scheme 1. Illustration of the Working Principle of (A) Au_x-GSH Sensitized TiO_2 Film As a Photoanode of PEC and (B) Au_x-GSH-Sensitized Pt/TiO_2 NPs Photocatalytic System for Water Splitting Reaction under Visible Light Illumination

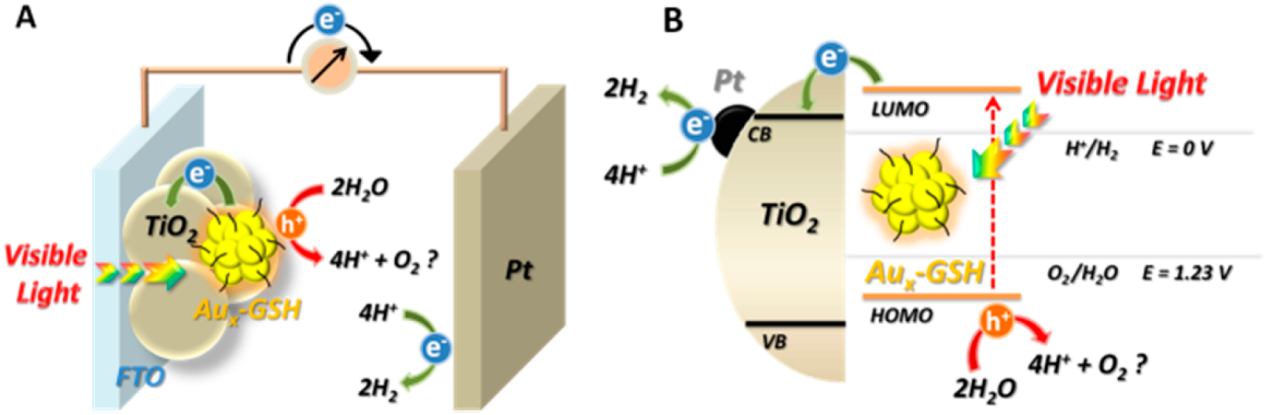

dx.doi.org/10.1021/ja5017365 | J. Am. Chem. Soc. 2014, 136, 6075−6082

$$Au_x - GSH^*\cdots TiO_2 \rightarrow Au_x - GSH^+\cdots TiO_2(e) \quad (2)$$

$$TiO_2(e) + Pt \rightarrow TiO_2 + Pt(e) \quad (3)$$

$$Pt(e) + H^+ \rightarrow 1/2H_2 \quad (4)$$

$$Au_x - GSH^+ + 1/2H_2O \rightarrow Au_x - GSH + 1/4O_2 + H^+ \quad (5)$$

$$Au_x - GSH^+ \xrightarrow{\text{accumulated holes}} Au_x - GSH^{y+} \quad (6)$$

Regeneration of the sensitizer can be aided by the introduction of a sacrificial electron donor, in this case EDTA (0.1 M), into the electrolyte. Since EDTA is an excellent electron donor, it reduces the oxidized sensitizer quite effectively (eq 7).

$$Au_x - GSH^+ + EDTA \rightarrow Au_x - GSH + \text{oxidized EDTA} \quad (7)$$

Figure 2B shows the photocurrent density of Au_x-GSH-sensitized TiO_2 photoanode (two-electrode PEC with N_2 saturated 0.1 M phosphate solution as electrolyte) recorded under visible light illumination (300 mW/cm^2 using a 420 nm cutoff filter) at short circuit conditions. The photocurrent response to on−off cycles of illumination is reproducible, although a small decrease in the initial magnitude of photocurrent was noted with subsequent illuminations. This effect is most pronounced without EDTA present in the electrolyte. The photocurrent density attained ∼0.25 mA/cm^2 in the first cycle but decreased to ∼0.20 mA/cm^2 after three 30 s illumination cycles. This decrease is attributed to oxidation of the Au_x-GSH due to incomplete regeneration because of the slow water oxidation kinetics. A relatively stable and higher photocurrent was also observed when 0.1 M EDTA was presented in the electrolyte ((d) in Figure 2B). The initial decrease in photocurrent seen immediately after turning on the illumination is indicative of the fact that the mass transfer limitation associated with the diffusion of EDTA within the mesoscopic film plays an important role. Slower regeneration of the Au_x-GSH NC surface will increase the charge recombination rate and thus cause the decrease in the photocurrent. The photocurrent becomes steady once the steady state between the EDTA diffusion and interfacial charge transfer is achieved. The small residual current (<2%) upon stopping the illumination is likely to arise from the discharge of accumulated charges near the anode.

While photocurrent is an important indicator in such photoelectrochemical systems, it does not necessarily correlate to H_2 production. Therefore, we correlated the observed photocurrent in a sealed PEC to the H_2 evolved at the counter electrode. The gas mixture in the headspace was periodically recorded via gas chromatography (GC) analysis while the photocurrent was continuously monitored. A large surface area (7.0 cm^2) photoanode was employed in a two electrode PEC with platinum counter electrode (see Figure S2 in the SI and Experimental Section for details). Figure 3A shows the photocurrent−time curve recorded following the illumination of visible light (λ > 420 nm). The maximum photocurrent of 0.63 mA quickly decreased to 0.27 mA within 10 min of illumination. The decrease in photocurrent was mainly associated with the detachment of Au_x-GSH NCs from the TiO_2 surface. This was independently confirmed from the absorption spectra of the electrolyte and photoanode following prolonged illumination (Figure S3B in the SI). The total charge passed through the external circuit was integrated over the course of the illumination and converted to moles of electrons. Dividing this value by the two electrons needed for H_2 production yields the maximum attainable Faradaic efficiency. Figure 3B shows the comparison of μmoles of electrons passed through the external circuit and the μmoles of hydrogen produced. In the absence of an external hole scavenger, we see 2 μmol of hydrogen production with a Faradaic efficiency of ∼65% during the hour-long period of illumination. We were not able to detect oxygen as a measurable product, and it is likely to be lower than the detection limit (<0.2 μmol from 40 μL of gas injection). It is likely that side reactions, including self-oxidation (eq 6), dominate the reactions at the anode. (Figure S3B in the SI shows changes in the absorption spectra of the electrode during the operation of PEC).

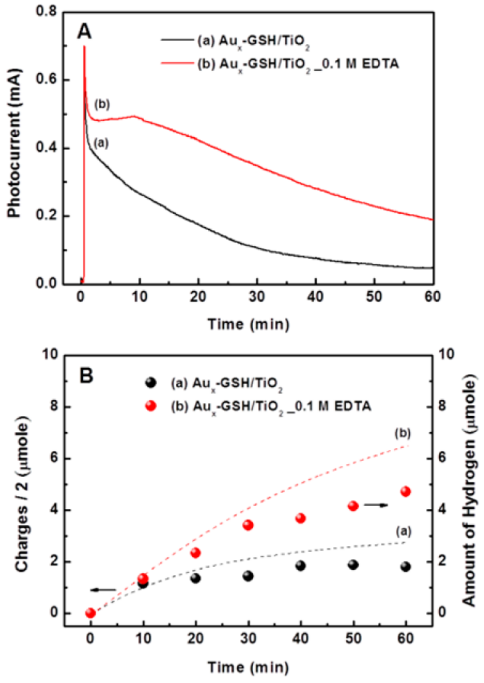

Figure 3. (A) Time course of photocurrent recorded from an Au_x-GSH-sensitized TiO_2 photoanode (area: 7 cm^2) in 0.1 M argon-saturated phosphate solution (pH = 7) (a) in the absence and (b) in the presence of 0.1 M EDTA. (B) Corresponding Coulometric time course trace obtained from the cumulative charge divided by two (dashed line). The amount of evolved hydrogen (dots) as measured by GC is plotted at different time intervals and used for evaluating Faradaic efficiency. Experimental conditions: two-electrode PEC setup employing Au_x-GSH-sensitized TiO_2 film as photoanode and platinum gauze as a counter electrode operated under short circuit conditions. Visible illumination was from a xenon lamp (>420 nm), 300 mW/cm^2. The pH of the electrolyte was adjusted to 7 with dilute NaOH.

When the electrolyte contained the sacrificial reagent, EDTA, an increased amount of charge flowed through the circuit which in turn resulted in the higher yields of hydrogen. The efficient scavenging of holes at the anode by EDTA suppresses charge recombination processes and thus increases the rate of H_2 production at the counter electrode. Nearly 3 times higher yields of H_2 (5 μmol) was observed in the presence of EDTA corresponded to the Faradaic efficiency of 72% during the 1 h illumination.

A three electrode PEC was also examined. The working electrode in this cell was held at a bias voltage of 0.4 V vs RHE

dx.doi.org/10.1021/ja5017365 | J. Am. Chem. Soc. 2014, 136, 6075−6082

and showed similar results as the two electrode cell, with relatively higher H_2 production. An image showing the H_2 generation from this three electrode cell in aqueous media (pH = 7.0) is shown in Figure 4, and a movie of this process is

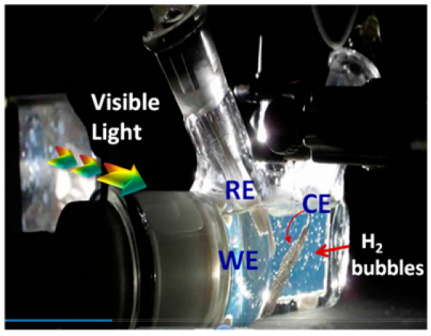

Figure 4. H_2 evolution at the Pt mesh counter electrode is shown in a three-electrode assembly in the absence of any hole scavenger. In this system a flat working electrode was illuminated with visible light at an applied bias potential of 0.4 V vs RHE. The electrode and cell configuration (Figure S2 in the SI) and a video clip showing the H_2 evolution is included in the SI.

shown in the SI (ja5017365_si_003.avi). The results showing the H_2 production at this applied bias in the absence of a hole scavenger is shown in Figure S4 in the SI. The direct correlation between the photoelectrochemical conversion of light into electricity and chemical energy (H_2 production) shows the effectiveness of Au_x-GSH NCs as a visible sensitizer for solar fuel generation.

Au_x-GSH/Pt/TiO_2 Photocatalytic Slurry System for Water Splitting Reaction. In addition to the previously discussed system, a photocatalytic slurry system consisting of Au_x-GSH/Pt/TiO_2 nanocomposite particles suspended in aqueous system in the absence and presence of sacrificial reagent was tested for hydrogen production. The working principle of this photocatalytic system is illustrated in Scheme 1B. The Au_x-GSH/Pt/TiO_2 nanocomposite was prepared first by depositing a controlled amount of Pt onto TiO_2 nanoparticles (NPs) by a photodeposition method.[41] This was followed by attaching Au_x-GSH NCs to the Pt/TiO_2 NPs. To complete this attachment, the suspensions of Pt/TiO_2 NPs are mixed with the Au_x-GSH NCs solution at pH = 4 and stirred for 4 h. (See Experimental Section for detailed experimental procedure.) TEM images of Pt/TiO_2 and Au_x-GSH/Pt/TiO_2 are shown in A and B of Figure 5, respectively. The TEM analysis in Figure 5A reveals a very low coverage of the TiO_2 NPs (~25 nm diameter) with the relatively smaller Pt NPs (~2.2 nm diameter). We deliberately maintained a low Pt loading to allow for deposition of the sensitizer on the TiO_2 surface. Upon deposition of Au_x-GSH NCs onto Pt/TiO_2 nanoparticles we observed a much denser coverage of the TiO_2 NPs (Figure 5B). The distribution of the Au_x-GSH NCs was uniform over the entire TiO_2 surface without significant aggregation. STEM-EDS spectral analysis (Figure 5D) confirmed the presence of Au_x-GSH NCs. The loading of Au_x-GSH NCs on Pt/TiO_2 NPs was estimated to be ~18 wt % by weighing the sample before and after sensitization.

Photocatalytic slurry experiments were initially performed in DI water (pH = 7.0, adjusted using dilute NaOH solution) under visible light illumination (λ > 420 nm). The headspace of the reaction cell was sampled periodically and injected into a

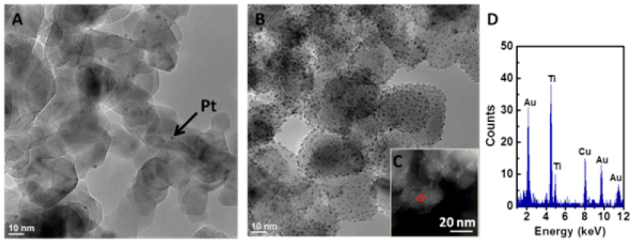

Figure 5. TEM images of (A) Pt/TiO_2 nanoparticles and (B) Au_x-GSH modified Pt/TiO_2 nanoparticles. (C) STEM image of Au_x-GSH modified Pt/TiO_2 NPs, and (D) STEM-EDS spectrum confirming the presence of Au_x-GSH in the highlighted region in (C). The arrow in (A) shows one of the Pt nanoparticles deposited on TiO_2.

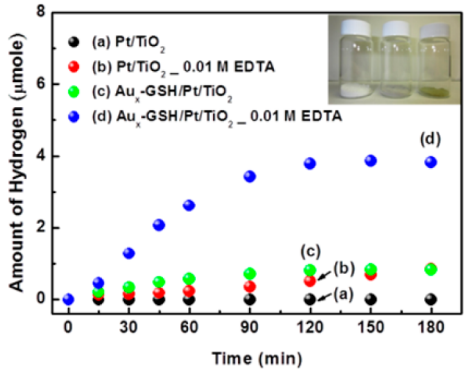

Figure 6. Time course of hydrogen evolution following the visible light illumination of an aqueous suspension containing (a) and (b) Pt/TiO_2 nanoparticles, and (c) and (d) Au_x-GSH-sensitized Pt/TiO_2 nanoparticles. The experiments were conducted in aqueous solution (pH 7) (a) and (c) in the absence and (c) and (d) presence of 0.01 M EDTA aqueous solution. Experimental conditions: 10 mg of 0.3 wt % Pt/TiO_2 nanoparticles or Au_x-GSH-sensitized 0.3 wt % Pt/TiO_2 nanoparticles in 4 mL argon-saturated solution. Visible illumination (300 mW/cm^2) is from a xenon lamp using a 420 nm cutoff filter. Inset shows a photograph of the TiO_2 (left), Pt/TiO_2 (middle) and Au_x-GSH-sensitized Pt/TiO_2 (right) powders that were suspended in solution for the photocatalysis experiments.

GC for H_2 analysis. Figure 6 shows the evolution of H_2 following the excitation of Au_x-GSH NCs deposited on Pt/TiO_2 NPs photocatalytic system. A linear increase in the amount of evolved hydrogen was observed over the first 90 min of the illumination. No hydrogen was detected when the Pt/TiO_2 NPs system was illuminated under similar experimental conditions (trace (*a*) in Figure 6), confirming that the Au_x-GSH NCs are responsible for the hydrogen generation. The rate of hydrogen evolution over the first 60 min is 0.3 mmol of hydrogen/h/g of Au_x-GSH NCs. Prolonged illumination (>120 min) decreased and eventually stopped hydrogen production, revealing the possible deactivation of Au_x-GSH NCs with extended illumination. When 0.01 M EDTA was introduced into the aqueous solution as a sacrificial electron donor, a significant increase in hydrogen production rate (1.4 mmol of hydrogen/h/g of Au_x-GSH NCs) was observed. As before, hydrogen evolution ceased with prolonged illumination (>120 min). Despite the presence of EDTA, the Au_x-GSH NCs did not remain active for an extended period. The apparent quantum yield (AQY) was measured using monochromatic 395 nm (broad band) illumination. The quantum yield of H_2 production for Au_x-GSH Sensitized Pt/TiO_2 NPs was 0.05%

dx.doi.org/10.1021/ja5017365 | J. Am. Chem. Soc. 2014, 136, 6075−6082

for water (pH = 7) and 0.13% for water containing of 0.01 M of EDTA.

The Au_x-GSH/Pt/TiO_2 nanocomposite was analyzed after performing the photocatalytic reaction by TEM. These TEM images (Figures S5 and S6 in the SI) reveal that the Au_x-GSH NCs aggregate into large NPs (~5 nm diameter) upon continuous illumination. This is consistent with previous results where it has been shown that metal nanoparticles deposited on TiO_2 undergo transformations during photoirradiation.[42] Additionally, metal NCs exposed to high-energy electron beams[43] or sintered at high temperature (>150 °C) also exhibit aggregation.[44] Therefore, we conclude that the observed lower activity of the Au_x-GSH/Pt/TiO_2 nanocomposite following prolonged irradiation stems from the morphological changes of the sensitizer. Capping of the clusters with a redox relay molecule or water oxidation catalyst could increase stability.

CONCLUDING REMARKS

In summary, the Au_x-GSH NCs are effective at extending the photoresponse of a large band gap semiconductor, such as TiO_2. Of particular interest is its ability to harvest visible photons for the purpose of hydrogen production through water splitting. Hydrogen evolution is observed in photoelectrochemical (PEC) and photocatalytic (slurry system) configurations and shows the versatility of this approach for converting light energy into a chemical fuel. Despite the promise of this approach, it is evident that the observed photoconversion efficiencies are quite low and require new strategies to boost both the performance and stability of the sensitizer. However, it should be noted that the majority of *high efficiency* claims in the literature involve either an applied bias or a sacrificial electron donor. The H_2 evolution experiments carried out in the present study using neutral water (pH = 7) and under no externally applied bias potential show the effectiveness of these thiolated gold clusters in generating solar fuels. Work is currently underway to synthesize differently sized gold clusters to extend the absorption further into the visible while retaining the same redox properties. Another approach would be to introduce plasmonic nanoparticles (e.g., Au_x-GSH NC-capped gold nanoparticles) and assess the visible activity reported for gold nanoparticles in the literature.

Despite our effort to probe the oxygen evolution, we were not able to identify O_2 as one of the products of the water-splitting reaction. Incorporating a water oxidation catalyst such as IrO_2 should be able facilitate the oxidation of water and produce oxygen. A relatively long-lived excited state (780 ns) and reversible redox properties make Au_x-GSH clusters a promising new class of photosensitizer. The ability to generate hydrogen under visible light irradiation without external bias represents the first step toward exploring their visible activity for solar fuel applications.

ASSOCIATED CONTENT

Supporting Information

Absorption and emission spectra of Au_x-GSH nanoclusters in solution, images of Au_x-GSH sensitized TiO_2 photoanode and photoelectrochemical cell (PEC) employed for hydrogen generation, images and absorption spectra of Au_x-GSH sensitized TiO_2 photoanode before and after performing hydrogen generation reaction, photocurrent and the corresponding hydrogen evolved during the course of irradiation in a three-electrode PEC under 0.4 V vs RHE, TEM images of Au_x-GSH/Pt/TiO_2 nanocomposite after performing photocatalytic reaction, and video of hydrogen generation reaction in a three-electrode PEC under 0.4 V vs RHE without EDTA. This material is available free of charge via the Internet at http://pubs.acs.org.

AUTHOR INFORMATION

Corresponding Author

pkamat@nd.edu

Notes

The authors declare no competing financial interest.

ACKNOWLEDGMENTS

The research described herein was supported by the Division of Chemical Sciences, Geosciences, and Biosciences, Office of Basic Energy Sciences of the U.S. Department of Energy, through award DE-FC02-04ER15533. This is contribution number NDRL No. 5010 from the Notre Dame Radiation Laboratory.

REFERENCES

(1) Chen, X.; Shen, S.; Guo, L.; Mao, S. S. *Chem. Rev.* **2010**, *110*, 6503.
(2) Kay, A.; Cesar, I.; Grätzel, M. *J. Am. Chem. Soc.* **2006**, *128*, 15714.
(3) Brillet, J.; Grätzel, M.; Sivula, K. *Nano Lett.* **2010**, *10*, 4155.
(4) Li, L.; Yu, Y.; Meng, F.; Tan, Y.; Hamers, R. J.; Jin, S. *Nano Lett.* **2012**, *12*, 724.
(5) Kho, Y. K.; Teoh, W. Y.; Iwase, A.; Mädler, L.; Kudo, A.; Amal, R. *ACS Appl. Mater. Interfaces* **2011**, *3*, 1997.
(6) Ng, Y. H.; Iwase, A.; Kudo, A.; Amal, R. *J. Phys. Chem. Lett.* **2010**, *1*, 2607.
(7) Warren, E. L.; Atwater, H. A.; Lewis, N. S. *J. Phys. Chem. C* **2014**, *118*, 747.
(8) Sasaki, Y.; Kato, H.; Kudo, A. *J. Am. Chem. Soc.* **2013**, *135*, 5441.
(9) Iwase, A.; Ng, Y. H.; Ishiguro, Y.; Kudo, A.; Amal, R. *J. Am. Chem. Soc.* **2011**, *133*, 11054.
(10) Maeda, K.; Lu, D.; Domen, K. *ACS Catal.* **2013**, *3*, 1026.
(11) Youngblood, W. J.; Lee, S.-H. A.; Maeda, K.; Mallouk, T. E. *Acc. Chem. Res.* **2009**, *42*, 1966.
(12) Youngblood, W. J.; Lee, S.-H. A.; Kobayashi, Y.; Hernandez-Pagan, E. A.; Hoertz, P. G.; Moore, T. A.; Moore, A. L.; Gust, D.; Mallouk, T. E. *J. Am. Chem. Soc.* **2009**, *131*, 926.
(13) Gao, Y.; Ding, X.; Liu, J.; Wang, L.; Lu, Z.; Li, L.; Sun, L. *J. Am. Chem. Soc.* **2013**, *135*, 4219.
(14) Brimblecombe, R.; Koo, A.; Dismukes, G. C.; Swiegers, G. F.; Spiccia, L. *J. Am. Chem. Soc.* **2010**, *132*, 2892.
(15) Jin, R. *Nanoscale* **2010**, *2*, 343.
(16) Chen, Y.-S.; Choi, H.; Kamat, P. V. *J. Am. Chem. Soc.* **2013**, *135*, 8822.
(17) Stamplecoskie, K. G.; Chen, Y.-S.; Kamat, P. V. *J. Phys. Chem. C* **2013**, *118*, 1370.
(18) Chen, W.-T.; Hsu, Y.-J.; Kamat, P. V. *J. Phys. Chem. Lett.* **2012**, *3*, 2493.
(19) Negishi, Y.; Iwai, T.; Ide, M. *Chem. Commun.* **2010**, *46*, 4713.
(20) Fields-Zinna, C. A.; Crowe, M. C.; Dass, A.; Weaver, J. E. F.; Murray, R. W. *Langmuir* **2009**, *25*, 7704.
(21) Negishi, Y.; Nobusada, K.; Tsukuda, T. *J. Am. Chem. Soc.* **2005**, *127*, 5261.
(22) Zheng, J.; Zhang, C.; Dickson, R. *Phys. Rev. Lett.* **2004**, *93*, 077402.
(23) Negishi, Y.; Sakamoto, C.; Ohyama, T.; Tsukuda, T. *J. Phys. Chem. Lett.* **2012**, *3*, 1624.
(24) Yu, Y.; Chen, X.; Yao, Q.; Yu, Y.; Yan, N.; Xie, J. *Chem. Mater.* **2013**, *25*, 946.
(25) Wu, Z.; Jin, R. *Nano Lett.* **2010**, *10*, 2568.

(26) Azcárate, J. C.; Corthey, G.; Pensa, E.; Vericat, C.; Fonticelli, M. H.; Salvarezza, R. C.; Carro, P. *J. Phys. Chem. Lett.* **2013**, *4*, 3127.
(27) Herzing, A. A.; Kiely, C. J.; Carley, A. F.; Landon, P.; Hutchings, G. J. *Science* **2008**, *321*, 1331.
(28) Valden, M. *Science* **1998**, *281*, 1647.
(29) Kauffman, D. R.; Alfonso, D.; Matranga, C.; Li, G.; Jin, R. *J. Phys. Chem. Lett.* **2013**, *4*, 195.
(30) Oliver-Meseguer, J.; Cabrero-Antonino, J. R.; Domínguez, I.; Leyva-Pérez, A.; Corma, A. *Science* **2012**, *338*, 1452.
(31) Gao, Y.; Shao, N.; Pei, Y.; Chen, Z.; Zeng, X. C. *ACS Nano* **2011**, *5*, 7818.
(32) Lopez-Acevedo, O.; Kacprzak, K. A.; Akola, J.; Häkkinen, H. *Nat. Chem.* **2010**, *2*, 329.
(33) Corma, A.; Concepción, P.; Boronat, M.; Sabater, M. J.; Navas, J.; Yacaman, M. J.; Larios, E.; Posadas, A.; López-Quintela, M. A.; Buceta, D.; Mendoza, E.; Guilera, G.; Mayoral, A. *Nat. Chem.* **2013**, *5*, 775.
(34) Yu, C.; Li, G.; Kumar, S.; Kawasaki, H.; Jin, R. *J. Phys. Chem. Lett.* **2013**, *4*, 2847.
(35) Luo, Z.; Yuan, X.; Yu, Y.; Zhang, Q.; Leong, D. T.; Lee, J. Y.; Xie, J. *J. Am. Chem. Soc.* **2012**, *134*, 16662.
(36) Sakai, N.; Tatsuma, T. *Adv. Mater.* **2010**, *22*, 3185.
(37) Archer, M. D.; Bolton, J. R. *J. Phys. Chem.* **1990**, *94*, 8028.
(38) De Lasa, H. I.; Serrano Rosales, B.; Navarro, R. M.; del Valle, F.; Villoria de la Mano, J. A.; Álvarez-Galván, M. C.; Fierro, J. L. G. *Adv. Chem. Eng.* **2009**, *36*, 111.
(39) Swanick, K. N.; Hesari, M.; Workentin, M. S.; Ding, Z. *J. Am. Chem. Soc.* **2012**, *134*, 15205.
(40) Lee, D.; Donkers, R. L.; Wang, G.; Harper, A. S.; Murray, R. W. *J. Am. Chem. Soc.* **2004**, *126*, 6193.
(41) Zhang, J.; Xu, Q.; Feng, Z.; Li, M.; Li, C. *Angew. Chem., Int. Ed.* **2008**, *47*, 1766.
(42) Lahiri, D.; Subramanian, V.; Shibata, T.; Wolf, E. E.; Bunker, B. A.; Kamat, P. V. *J. Appl. Phys.* **2003**, *93*, 2575.
(43) Ramasamy, P.; Guha, S.; Shibu, E. S.; Sreeprasad, T. S.; Bag, S.; Banerjee, A.; Pradeep, T. *J. Mater. Chem.* **2009**, *19*, 8456.
(44) Smith, B. L.; Hutchison, J. E. *J. Phys. Chem. C* **2013**, *117*, 25127.